Atomic-Scale Analysis of the Solvation Thermodynamics of Hydrophobic Hydration

Stewart R. Durell* and Anders Wallqvist#

*Laboratory of Mathematical Biology, National Cancer Institute, National Institutes of Health, Bethesda 20892, and #Laboratory of Mathematical Biology, Science Applications International Corporation—Frederick, National Cancer Institute–Frederick Cancer Research and Development Center, Frederick, Maryland 21702, USA

ABSTRACT Molecular dynamics simulations are used to model the transfer thermodynamics of krypton from the gas phase into water. Extra long, nanosecond simulations are required to reduce the statistical uncertainty of the calculated "solvation" enthalpy to an acceptable level. Thermodynamic integration is used to calculate the "solvation" free energy, which together with the enthalpy is used to calculate the "solvation" entropy. A comparison series of simulations are conducted using a single Lennard-Jones sphere model of water to identify the contribution of hydrogen bonding to the thermodynamic quantities. In contrast to the classical "iceberg" model of hydrophobic hydration, the favorable enthalpy change for the transfer process at room temperature is found to be due primarily to the strong van der Waals interaction between the solute and solvent. Although some stabilization of hydrogen bonding does occur in the solvation shell, this is overshadowed by a destabilization due to packing constraints. Similarly, whereas some of the unfavorable change in entropy is attributed to the reduced rotational motion of the solvation shell waters, the major component is due to a decrease in the number of positional arrangements associated with the translational motions.

INTRODUCTION

It is generally recognized that the "hydrophobic effect" plays an important role in determining the structure and function of biomolecules (Ravishanker and Beveridge, 1986; Dill, 1990; Blokzijl and Engberts, 1993). For example, the tendency of nonpolar amino acid residues to avoid water causes them to aggregate and form the cores of proteins. Likewise, the association of subunits and the binding of substrates often occur at nonpolar patches on the surfaces of the molecules (Young et al., 1994). To understand the basis of the hydrophobic effect, considerable work has gone into measuring the thermodynamics of model systems, such as the transfer of small nonpolar atoms from the gas phase into water. Because of the unique properties, the aqueous solvation of nonpolar solutes is given the special name of "hydrophobic hydration." In this study we focus on the transfer thermodynamics obtained for the noble gas atom krypton (Table 1). At room temperature (300°K), this is characterized by a large reduction in both enthalpy (which is favorable) and entropy (which is unfavorable). This is in contrast to the transfer into a typical nonpolar solvent, in which the magnitudes of these changes are considerably less. As is typical for hydrophobic hydration, the unfavorable entropy term dominates and causes a positive free energy change for the reaction. This, of course, is responsible for the well-known low solubility for nonpolar solutes in water. However, as seen in Table 1, both the enthalpy and entropy changes have a strong temperature dependence, becoming more positive at higher temperatures. Interestingly, these effects tend to compensate, giving a near-constant free energy change over a broad range of temperatures. In addition, the steep temperature dependence of the enthalpy change is what is responsible for the large partial molar heat capacity of the solute, which is also a well-recognized feature of hydrophobic hydration.

Perhaps the first, and most enduring, molecular explanation for the unique thermodynamics of "hydrophobic hydration" is the "iceberg" model proposed by Frank and Evans (1945). Accordingly, the water molecules of the solvation shell are postulated to form a "microscopic iceberg," which accommodates the larger cavity size required by the solute. However, despite the allusion to ice, the exact structure of these "frozen patches" is not specified, and they are simply regarded as regions of "greater crystallinity." In this case, then, the more favorable change in enthalpy for the solvation process is attributed to an enhancement of the hydrogen bond interactions in the "iceberg" structure, and the more unfavorable decrease in entropy is attributed to the subsequent reduced mobility of the water molecules. Similarly, the relatively large reduction in the negative magnitudes of the transfer enthalpy and entropy with increasing temperature (i.e., the steep temperature dependence) is explained by there being smaller "icebergs" formed when there is greater disruptive thermal motion. Despite the ambiguities, the concept of "structure enhancement" has had a profound influence on the thinking concerning hydrophobic phenomena, being the root of numerous experimental and theoretical investigations (Holtzer and Emerson, 1969; Ravishanker

Received for publication 1 April 1996 and in final form 11 July 1996.

Address reprint requests to Dr. Stewart R. Durell, Laboratory of Mathematical Biology, NCI/NIH, Bldg. 12B, Rm. B116, 12 South Dr., Bethesda, MD 20842-5677. Tel.: 301-496-2394; Fax: 301-402-4724; E-mail: durell@helix.nih.gov.

0006-3495/96/10/1695/12 $2.00

TABLE 1 Experimental "solvation" thermodynamics: quantities for krypton in water at 1 atm

Temp. (K)	ΔG^*_{Kr} (kcal/mol)	ΔH^*_{Kr} (kcal/mol)	ΔS^*_{Kr} (cal/mol/K)
300.0	1.68	−3.27	−16.5
325.0	2.03	−1.87	−12.0
350.0	2.28	−0.70	−8.5

The data are linear interpolations from the values at 25°C, 50°C, and 75°C from Ben-Naim (1987, 1992), which are derived from Crovetto *et al.* (1982).

and Beveridge, 1986; Dill, 1990; Blokzijl and Engberts, 1993).

A major step forward occurred in the mid to late 1970s with the increased availability of computers capable of simulating aqueous solutions at atomic detail (Ravishanker and Beveridge, 1986; Blokzijl and Engberts, 1993). With Monte Carlo and/or molecular dynamics methods it became possible to characterize the effect of a nonpolar solute on the surrounding water molecules (Zichi and Rossky, 1985, 1986). Indeed, most studies have seemed to confirm the existence of "enhanced structure," as a nonrandom net orientation is usually observed for the waters in the solvation shell. For example, in the first shell the waters tend to have their O-H bonds tangential to the surface of the solute, whereas in the second shell the O-H bonds tend to point toward the solute. Although not completely "frozen," some studies have also found a reduction of as much as 30% in the translational and rotational motion of the waters in the "iceberg." In contrast, however, dissenting views have emerged about the specific molecular effects responsible for the unusual thermodynamic changes. Whereas some studies have found an increase in the number and lifetime of the hydrogen bonds in the solvation shell (Blokzijl and Engberts, 1993), another study indicates that it is mostly the solute-solvent interaction that accounts for the more favorable enthalpy change for the solvation process (Jorgensen et al., 1985). Similarly, the results of Madan and Lee (1994) contradict the notion that it is the induced orientation and changes in the hydrogen bonding structure of the solvation shell waters that cause the unfavorable entropy (and thus free energy) changes. Although these studies have used slightly different systems and potential energy functions, most of the dispute over the thermodynamics is due to the relatively high degree of statistical uncertainty in the calculated results. This is because the changes in energy for the solvation process tend to be very small compared to the total energy of the system.

Consequently, one main purpose of this work is to increase the accuracy of the enthalpy and entropy calculations. This will aid us in determining the contributions of different molecular effects to the unique thermodynamics of the transfer process and hydrophobic hydration. The strategy used to decrease the statistical uncertainty in the calculations is simply to increase the length of the simulation, and thus increase the number of independent samples. To the best of our knowledge, the 1-ns-long molecular dynamics trajectories used here represent at least a fourfold increase in sampling compared to previous studies of this type. As described above, krypton was chosen as the model nonpolar solute for the transfer reaction ($Kr_g \rightarrow Kr_{aq}$), for which there are a number of advantages. The first is that there are ample experimental data for comparison (Table 1), and extensive work has gone into parameterizing the interaction energy with water (Swope and Andersen, 1984). The second is that the ~4.5-Å diameter of krypton is significantly larger than the ≤3.1-Å range of cavities found in bulk water (Pratt and Pohorille, 1992; Forsman and Jönsson, 1994; Madan and Lee, 1994), thus enhancing the amount of "structural" perturbation of the solvent. The third is that a single-atom solute model avoids having to exhaustively sample conformational isomers, and provides a natural spherical symmetry for averaging the distance-dependent effects on the waters. Finally, a parallel series of simulations is conducted using a single Lennard-Jones sphere analog of water to identify the contribution of hydrogen bonding to the thermodynamic results.

METHODS

Statistical thermodynamics formalism

Perhaps the most appropriate form for comparison with molecular dynamics simulations is the expression of the experimental data in terms of the "solvation" quantities defined by Ben-Naim (1987, 1992). In short, these are calculated from the number densities at equilibrium of the solute (solvation) in the two mediums or phases of the transfer process. In contrast to an arbitrary standard state, the "solvation" quantities are for the specific set of environmental conditions (e.g., temperature, pressure, and composition) under which the experimental measurements are made. At the atomic level, they reflect the coupling work or molecular interactions between the solute and its environment. Because krypton is sparsely soluble in water under the conditions of temperature and pressure used to obtain the data in Table 1, the composition of the solute in the liquid can be taken to be at the limit of infinite dilution. This is convenient for the simulations, because a single solute allows us to avoid calculating an ensemble average for the interaction energy with other solutes (which would require considerably more computer time to sample a representative population of solute-solute configurations). Because any contribution due to the solute's momentum is absent from the "solvation" therodynamic quantities, its position is kept fixed in the fluid simulations.

Although it is typically difficult to calculate thermodynamic partition functions for molecular liquids, it is possible to derive ensemble-average expressions for the "solvation" quantities that can be solved by molecular dynamics or Monte Carlo sampling methods (Ben-Naim, 1987, 1992; Mezei and Beveridge, 1986; Beveridge and DiCapua, 1989). Perhaps the simplest is for the "solvation" enthalpy

(ΔH^*_{Kr}), which is just the difference in potential energy between the solution and pure water systems:

$$\Delta H^*_{Kr} \approx (\langle B_{Kr-w}\rangle_{soln} + \langle U_{w-w}\rangle_{soln}) - \langle U_{w-w}\rangle_{pure} \quad (1)$$

$$= \langle B_{Kr-w}\rangle_{soln} + \langle \Delta U_{w-w}\rangle_{soln-pure}.$$

In Eq. 1, $\langle B_{Kr-w}\rangle_{soln}$ is the average interaction, or "binding" energy, of the krypton with the water molecules in the Kr-containing solution; $\langle U_{w-w}\rangle_{soln}$ and $\langle U_{w-w}\rangle_{pure}$ are the average water-water interaction energies in the Kr-containing and pure water systems; and $\langle \Delta U_{w-w}\rangle_{soln-pure}$ is the average change in water-water interaction energy due to the addition of the solute (which is also known as the water "reorganization" energy). The first equality is only approximate because it neglects the mechanical $P\Delta V^*_{Kr}$ term, which is negligible at regular atmospheric pressures (Ben-Naim, 1987, 1992). (It should be noted that Eq. 1 is similar to an expression given by Jorgensen et al., 1985.)

Unlike the "solvation" enthalpy, the basic statistical mechanics expression for the "solvation" free energy (i.e., $\Delta G^*_{Kr} = -k_b T \ln\langle e^{(-B_{Kr-w}/k_b T)}\rangle_{pure}$) (Ben-Naim, 1987, 1992) cannot be evaluated directly by molecular dynamics simulation. Instead, the method of thermodynamic integration was employed, in which a coupling parameter (λ) is used to incrementally "grow" the solute in the system (Mezei and Beveridge, 1986; Beveridge and DiCapua, 1989). This is affected by making the solute-solvent "binding" term of the potential energy function vary as a function of the coupling parameter ($B(\lambda)$), such that there is no interaction when λ equals 0 and full interaction when λ equals 1. As described by Eq. 2, the "solvation" free energy is calculated by integrating the λ-dependent ensemble average of the partial λ derivative of the solute-solvent binding energy over λ:

$$\Delta G^*_{Kr} = \int_0^1 \left\langle \frac{\partial B(\lambda)}{\partial \lambda} \right\rangle_\lambda d\lambda. \quad (2)$$

It should be noted that the water-water interaction term of the potential energy function remains independent of λ and thus is absent from the derivative equation. This generally results in a smaller fluctuation than for the total potential energy of the system, which enables less sampling to obtain a statistically significant average value. However, the solute's effect on the water-water interaction still enters into the calculated free energy through the perturbed ensemble of water configurations over which the average is calculated.

Finally, the "solvation" entropy is calculated from the free energy and enthalpy using the fundamental thermodynamic relation given in Eq. 3:

$$\Delta S^*_{Kr} = \frac{\Delta H^*_{Kr} - \Delta G^*_{Kr}}{T}. \quad (3)$$

Computational details

Molecular dynamics simulations were conducted for both pure water (i.e., bulk phase) and an infinitely dilute krypton-containing solution (i.e., only one solute molecule present) at 300°K. For both systems, 214 water molecules were used in a cubic box with periodic image boundary conditions. For the solution, the position of the krypton was fixed at the center of the box to correspond with Ben-Naim's (1987, 1992) "solvation" formalism (see above). For the pure system the box volume was set to 6401.7 Å^3, which gives a density similar to that of real water at the same temperature and 1 atm pressure. For the solution system two parallel simulations were performed: 1) with the same box size, to represent a constant volume solvation process, and 2) with the box size increased, to account for the solute and represent a constant-pressure process. In the latter case the volume of the box was increased by 48.74 Å^3, which was simply obtained from the 2.26 Å van der Waals (VDW) radius used for the krypton atom (see below). It should be noted that for the constant-volume system the presence of the krypton actually causes a reduction in the space available to the water molecules.

All of the simulations were run using two distinctive models for the water molecules. These were the three-point TIPS3P model, which has both electrostatic and VDW interaction energy terms, and the single-point Lennard-Jones (LJ) model, which has only a VDW-type interaction. TIPS3P, which is included in the CHARMM software package (Brooks et al., 1983), is based on the TIP3P model developed by Jorgensen et al. (1983). The main difference is the addition of VDW terms for the hydrogens to prevent overlap with other atoms. The charges on the oxygen and each hydrogen atom are $-0.834e$ and $0.417e$, respectively. During the dynamics simulations, the SHAKE algorithm (Allen and Tildesley, 1987) was used to fix the O-H bond lengths and H-O-H bond angles to 0.96 Å and 104.5°. The LJ model was developed to serve as a reference to the TIPS3P liquid that lacks hydrogen bond interactions. As such, the Lennard-Jones parameters were adjusted in an attempt to best reproduce the pressure of the TIPS3P system at the same set density and temperature (see above). This involved making the interaction energy (ϵ) more favorable and decreasing the equilibrium separation distance (R_{min}), which can be thought of as a spherically symmetrical substitute for the effect of the strongly attractive hydrogen bonds among regular water molecules. The mass was also set to that of the TIPS3P molecule (i.e., 18.0154 amu). Similar models have been used by Pratt and Pohorille (1992), Madan and Lee (1994), and Wallqvist and Covell (1996). The krypton atom was also modeled as a single VDW shpere. In this case, the Lennard-Jones parameters developed by Swope and Andersen (1984) were used for the interaction with both the TIPS3P and LJ water molecules. Table 2 lists the Lennard-Jones parameters used for all relevant pairwise atomic interactions. Note that the krypton does not interact with the hydrogens of the TIPS3P waters.

TABLE 2 Pairwise Lennard-Jones parameters for krypton, TIPS3P, and LJ water models

Atom pairs	ϵ (kcal/mol)	R_{min} (Å)
TIPS3P waters		
O-O	−0.1521	3.537
O-H	−0.0836	1.993
H-H	−0.0460	0.449
Kr-O	−0.3950	3.860
Kr-H	0.0	—
LJ waters		
O-O	−0.5610	2.860
Kr-O	−0.3950	3.860

The TIPS3P values are from the CHARMM software package, the parameters for the krypton atom are from Swope and Andersen (1984), and the LJ water parameters were obtained as described in the text. Note that there is no Lennard-Jones interaction for the krypton with the TIPS3P hydrogens. For the Lennard-Jones potential of the form $A/r^{12} - C/r^6$, $A = \epsilon R_{min}^{12}$, $C = 2\epsilon R_{min}^6$, and $R_{min} = 2^{1/6}\sigma$.

The CHARMM computer program (Brooks et al., 1983) was used to perform the molecular dynamics simulations on a Cray YMP supercomputer. A typical performance was approximately 2 min/ps for the 214 water molecules of the pure TIPS3P system. As alluded to above, the systems were run under conditions of constant volume and temperature (NVT), which corresponds to the canonical ensemble. The Langevin algorithm (Pastor et al., 1988), with a frictional constant of 10 ps^{-1}, was used to heat and maintain the system's temperature by stochastically coupling the water molecules to a virtual heat bath. An integration time step of 1.0 fs was used, and coordinates were saved every 50 fs. Typically, 20 ps was used for heating and equilibration, and then sampling was conducted for the next 1000 ps for the TIPS3P systems, and for the next 600 ps for the LJ water systems. Nonbonded energies and forces were shifted to zero for atom separation distances of ≥8.5 Å using the FSHIFT (force-shifted or shifted-force) method for the electrostatic interactions, and the VSHIFT method for the VDW interactions (which is contained in contemporary versions of CHARMM) (Steinbach and Brooks, 1994; Allen and Tildesley, 1987; Haile, 1992). For truncating the electrostatic interactions, Prevost et al. (1990) found FSHIFT ($S(r) = (1 - r/r_c)^2$) to be superior to the original shift method in CHARMM ($S(r) = (1 - (r/r_c)^2)^2$) for reproducing the structural and dynamical properties of water calculated using Ewald summation (which includes all long-range interactions) (see also Wallqvist and Teleman, 1991; Wallqvist and Berne, 1993). The VSHIFT method adds $Cr^6 + D$ to the Lennard-Jones potential, where

$$C = 2\epsilon\left(\frac{R_{min}}{r_c}\right)^{12}\left(\frac{1}{r_c^6} - \frac{1}{R_{min}^6}\right), \quad D = \epsilon\left[4\left(\frac{R_{min}}{r_c}\right)^6 - 3\left(\frac{R_{min}}{r_c}\right)^{12}\right],$$

r is the separation distance between atoms, and r_c is the cutoff distance.

Free energy calculations

As described above, ΔG^*_{Kr} was calculated by the method of thermodynamic integration (Eq. 2) (Mezei and Beveridge, 1986; Beveridge and DiCapua, 1989). The integrand was approximated by calculating ensemble averages at discrete, intermediary values of λ. Except where noted, these were at 0.1 intervals between 0.0 and 1.0. Each average value was calculated from a separate 200-ps trajectory. Subsequently, the integration over λ was calculated using the trapezoidal rule and/or direct calculation of the trapezoidal areas between successive λ values. All free energy simulations were conducted at the constant volume of the pure liquid system. Because they are estimated to differ by no more than 0.7×10^{-3} kcal/mol (Ben-Naim, 1987, 1992) (which is considerably less than the statistical uncertainty), the "solvation" free energy at constant pressure was taken to be the same as the constant-volume result.

The procedure was carried out using four separate functional forms for the λ dependency of the solute-solvent "binding" energy (also known as "paths") (Eq. 4). The first three are nonlinear polynomial paths described by Resat and Mezei (1993), in which differing powers of λ are used to scale the repulsive (A/r^{12}) and attractive (C/r^6) terms of the Lennard-Jones potential (see also Mezei, 1992, 1993). The fourth is the separation-shifted scaled path described by Zacharias et al. (1994), with the modification that the solute grows instead of shrinks with increasing λ (to be consistent with the other three).

$$B(\lambda)_1 = \lambda^4 \frac{A}{r^{12}} - \lambda^3 \frac{C}{r^6} + \text{vshift}(\lambda)$$

$$\equiv \epsilon(\lambda) = \lambda^2\epsilon,\ R_{min}(\lambda) = \lambda^{\frac{1}{6}} R_{min} \tag{4a}$$

$$B(\lambda)_2 = \lambda^8 \frac{A}{r^{12}} - \lambda^6 \frac{C}{r^6} + \text{vshift}(\lambda)$$

$$\equiv \epsilon(\lambda) = \lambda^4\epsilon,\ R_{min}(\lambda) = \lambda^{\frac{1}{3}} R_{min} \tag{4b}$$

$$B(\lambda)_3 = \lambda^{40} \frac{A}{r^{12}} - \lambda^{22} \frac{C}{r^6} + \text{vshift}(\lambda)$$

$$\equiv \epsilon(\lambda) = \lambda^4\epsilon, \quad R_{min}(\lambda) = \lambda^3 R_{min} \tag{4c}$$

$$B(\lambda)_4 = \lambda \frac{A}{(r^2 + (1-\lambda)\delta)^6} - \lambda \frac{C}{(r^2 + (1-\lambda)\delta)^3} + \text{vshift}(\lambda). \tag{4d}$$

In Eq. 4, $A = \epsilon R_{min}^{12}$, $C = 2\epsilon R_{min}^6$, ϵ and R_{min} are the Lennard-Jones parameters listed in Table 2 for the krypton-water oxygen interaction, r is the separation distance, and δ is the separation-shift parameter. As recommended (Zacharias et al., 1994), δ was set to the square of the van der Waals radius of the krypton atom, which equals 5.1076 $Å^2$. The partial derivatives of the solute-solvent binding

energy with respect to λ (Eq. 2) were calculated analytically from the potential energy functions. It should be noted that the VSHIFT term is also a function of $\epsilon(\lambda)$, $R_{min}(\lambda)$ and $(r^2 + (1 - \lambda)\delta)$ (Eq. 4d), and therefore must be included to calculate the derivative. Because the free energy is a thermodynamic state variable, integration over the four different paths is expected to yield the same result, which is exploited as an internal test of the calculations.

In selecting a path it is important that the integrand be bounded over the interval of integration, and that there not be extreme, rapid changes that would require sampling at a prohibitively large number of intermediary λ values (Cross, 1986). For example, it is well known that for systems such as this, in which a particle is created in a dense medium, a simple linear path results in a divergence at the limit of $\lambda = 0$ (at which r can also equal zero) (Mezei and Beveridge, 1986; Beveridge and DiCapua, 1989). It has been rigorously shown that for potential functions of the form λ^α/r^n (such as Eqs. 4a–c), the limiting behavior of the integrand of Eq. 2 as λ goes to zero is $\lambda^{3\alpha/n-1}$ in three-dimensional space (Simonson, 1993; Resat and Mezei, 1994). Thus, for the polynomial paths of Eq. 4, which are dominated by the repulsive, A/r^{12} term at small r, bounded integrands are obtained when the exponent of the λ coefficient of that term is ≥4.0 (Mezei, 1992; Resat and Mezei, 1993; Simonson, 1993). As confirmed by Fleischman and Zichi (1991), when this exponent equals 4 the integrand converges to a positive value, and when it is greater than 4 it converges to zero. It has also been noted that when this exponent is the lowest value necessary to provide convergence, the volume of the solute scales linearly with λ and the integrand becomes more linear (Resat and Mezei, 1993). Thus, the first polynomial path, with λ^4 as the coefficient of the repulsive term, was selected to take advantage of the near-linear form of the integrand, which reduces the error in the quadrature approximation of the integral. To test the convergence of this path at small λ, the second and third polynomial paths were designed to increase the rate at which the solute shrinks. As can be seen, this is achieved by increasing the power of the first λ to 8 and 40, which provides a progressively smaller scaling factor with which the repulsive term is attenuated. The fourth path was selected because it utilizes an alternative mechanism for avoiding the end-point convergence problem (i.e., shifting the separation distance) and thus provides a more stringent test of the path independence of the calculated free energy value.

Statistical error analysis

As described by Allen and Tildesly (1987), the statistical uncertainty in the trajectory average of any observable value ($\sigma_{\langle E\rangle}$) can be calculated from the variance (σ_E^2) of that value and the number of independent samples, i.e.,

$$\sigma_{\langle E\rangle} = \sqrt{2\frac{\tau}{t}\sigma_E^2}, \tag{5}$$

where τ is the relaxation time, t is the time length of the trajectory, and the variance σ_E^2 equals $\langle(E_i - \bar{E})^2\rangle$. The relaxation time was calculated from the integral of the square of the normalized autocorrelation function ($\hat{c}(t')$), i.e.,

$$\tau = 2\int |\hat{c}(t')|^2\, dt', \tag{6}$$

where t' is the lag time between samples, $\hat{c}(t') = \langle\delta E(t')\delta E\rangle/\langle\delta E^2\rangle$, and $\delta E = (E_i - \bar{E})$. The value of the integral was evaluated numerically using the trapezoidal rule. As stated above, trajectory snapshots were recorded every 50 fs, which provides 20,000 not necessarily independent samples for a 1000-ps run. The calculated uncertainty is reported as $\pm 2\sigma$, which corresponds to the 95% confidence range. The uncertainty for the sum or difference of two numbers was calculated from the sum of the variances (i.e., $\sigma_{A\pm B}^2 = \sigma_A^2 + \sigma_B^2$).

RESULTS

To compare simulation results using the TIPS3P and LJ water models it is important to know how similar the liquid structures are that they produce. Accordingly, Fig. 1 *A* shows the water-water radial distribution function ($g(r)_{w-w}$) for the two models, obtained from the pure water systems at 300°K and a density of ~1 g/ml. Although both models display first and second peaks at approximately 2.8 and 5.5 Å, the magnitudes and widths are found to differ significantly. In particular, the TIPS3P liquid has a greater maximum at 2.85 Å, but a less pronounced minimum and second peak structure. Thus, despite the parameter changes in the LJ water model to obtain the same effective size (see Methods and Table 2), the pseudotetrahedral nature of the hydrogen bonds of the TIPS3P model causes an enhanced stabilization for the waters that are closest to each other at the expense of waters that are further apart (i.e., at the second peak). From the limiting behavior of the mean square displacement as a function of lag time, the translational diffusion coefficients were calculated to be 0.25 Å²/ps for the TIPS3P model and 0.53 Å²/ps for the LJ water model. The first is in good agreement with the experimental value of 0.24 Å²/ps for water at the same temperature (Krynicki et al., 1978). The greater diffusion coefficient for the LJ water must be related to the differences in stability of the water-water interactions that is observed in $g(r)_{w-w}$.

Fig. 1 *B* compares the two krypton-water radial distribution functions ($g(r)_{Kr-w}$) obtained from the increased-volume krypton-containing systems used for the constant-pressure process. Both liquids have first and second peaks at ~3.8 and 6.5 Å, which define the positions of the solvation shells around the krypton atom; however, the height of the first peak and the position of the first minimum are found to differ. The fact that the density in the first shell is greater for the TIPS3P liquid is interesting, considering that both systems use the same potential energy function for the solute-solvent interaction (Table 2). Thus, this again must be due

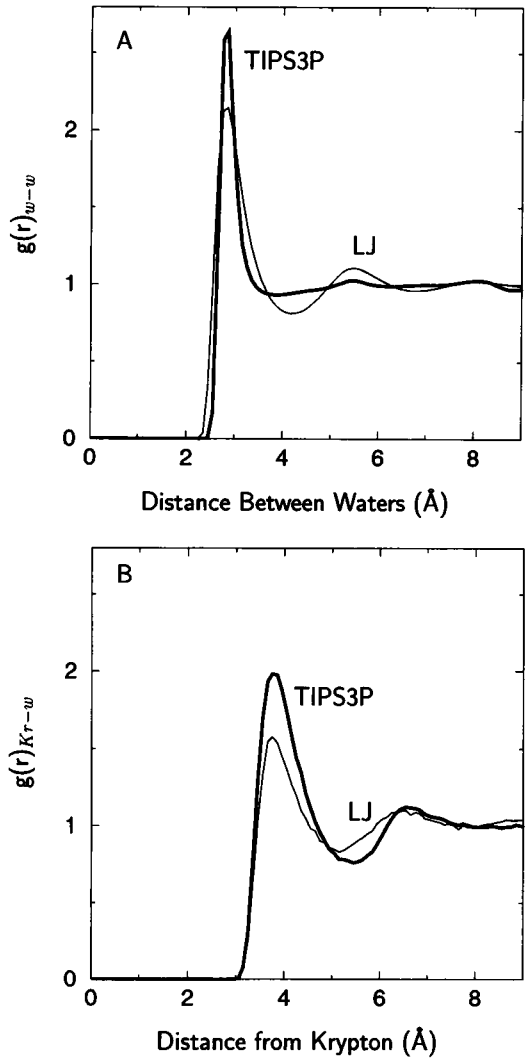

FIGURE 1 (*A*) Water-water ($g(r)_{w\text{-}w}$) and (*B*) krypton-water ($g(r)_{Kr-w}$) radial distribution functions of the TIPS3P (*thick*) and LJ (*thin*) water systems.

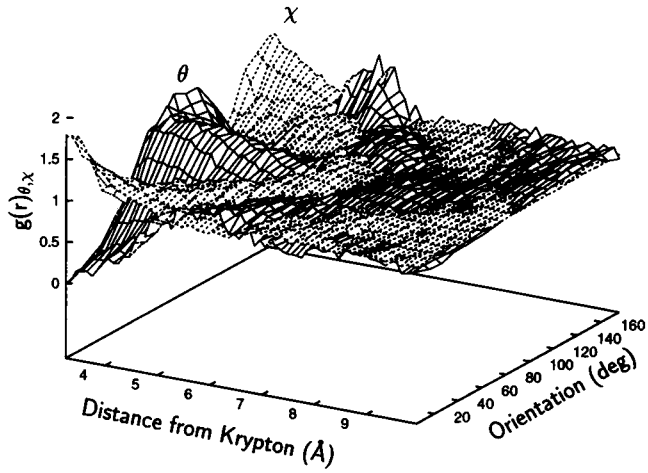

FIGURE 2 Orientational distributions of the TIPS3P waters as a function of distance from the krypton. θ (*solid mesh*) is the angle between the dipole moment of the water molecule and the solute-solvent position vector. Zero degrees corresponds to pointing radially away from the solute. χ (*dashed mesh*) is the angle between the vector conecting the two hydrogen atoms and the normal to the plane defined by the dipole moment and the solute-solvent position vector.

to the pseudotetrahedral nature of the hydrogen bond interactions between the TIPS3P water molecules. The same results are obtained for the Kr-containing systems used for the constant-volume process, except that the height of the first peak for the TIPS3P liquid is even 5% greater. Although partially counteracted by the greater density of LJ waters in the region between the two peaks, the running sum indicates a slightly greater number of TIPS3P molecules throughout the combined volume of the first and second solvation shells (data not shown). The maximum occurs at ~4.9 Å from the krypton atom, where there are an average of 2.6 more TIPS3P than LJ water molecules in the enclosed volume.

To further illustrate the effect on structure, Fig. 2 shows the distance dependence of the normalized distributions for the orientation angles θ and χ in the TIPS3P liquid. As described by Lazaridis and Paulaitis (1992), θ is the angle between the electrostatic dipole moment of the water molecule and the krypton-water position vector, and χ is the angle between the intrahydrogen vector and the normal to the plane formed by the two vectors used to define θ. From consideration of the geometry, it is seen that χ simply represents rotation around the dipole moment. For θ, 0° corresponds to the dipole moment pointing radially away from the krypton atom. At 3.8 Å, which is the density peak of the first solvation shell (Fig. 1 *B*), the maxima of the distributions are at 75° for theta, and 0° and 180° for χ. This corresponds to the O-H bond vectors being approximately tangential to the surface of the solute. In contrast, at 5.3 Å, which is between the first and second solvation shells, θ shifts to a maximum at ~180°, and χ becomes approximately uniform. This corresponds to the hydrogens pointing at an acute angle toward the solute. As also seen in the figure, the effect dies off at a distance of ~6 Å from the solute, and thus the waters at the peak of the second solvation shell (6.5 Å) have the same, random orientation as in the bulk phase. As described above, similar results have been observed in numerous other simulation studies using different solutes and water models (Blokzijl and Engberts, 1993).

Solvation enthalpy

Fig. 3 shows the running averages of the total potential energy of the volume adjusted Kr-containing and pure TIPS3P water systems at 300°K. Using the procedure described by Eq. 6, the relaxation time for each curve is calculated to be 225 fs. Thus, for a 1-ns trajectory, which corresponds to a million 1-fs time steps, there are only 4444 independent samples of the potential energy. The statistical variance (σ_E^2) of each curve is calculated to be approxi-

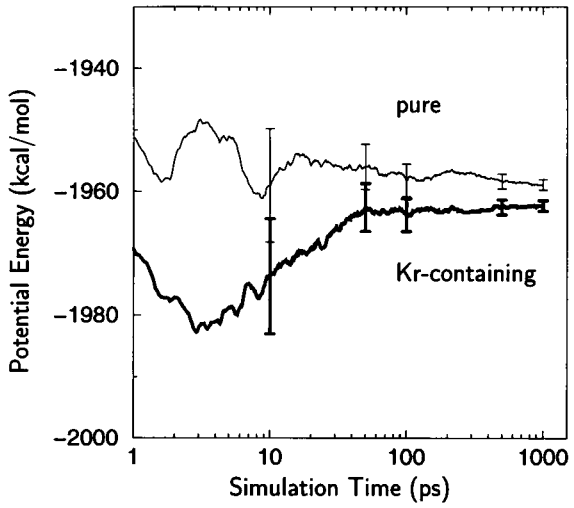

FIGURE 3 Running averages of the potential energy of the volume-adjusted krypton-containing (*thick*) and pure (*thin*) TIPS3P water systems. The error bars are $\pm 2\sigma$.

mately 401.5 (kcal/mol)^2. Thus, using Eq. 5, the 95% confidence range for the average potential energy ($\pm 2\sigma_{\langle E \rangle}$) is calculated to be 0.9 kcal/mol for both systems. For the "solvation" enthalpy (ΔH^*_{Kr}), which is the difference in average potential energy (Eq. 1), the statistical uncertainty is obtained from the square root of the sum of the variances (see Methods). This gives a 95% confidence range of ± 1.3 kcal/mol, which is 40% of the difference in the averages at 1 ns. Analysis of the LJ water systems revealed a similar relaxation time of 229 fs, but a much smaller variance of only 48.9 (kcal/mol)^2. This is due to the fact that the total potential energy is approximately 4.5 times smaller in magnitude than for the TIPS3P systems. Thus, for the 600-ps trajectories used for the LJ systems, the 95% confidence range for ΔH^*_{Kr} is calculated to be only ± 0.5 kcal/mol.

Fig. 4 *A* shows the ΔH^*_{Kr} calculated for the TIPS3P systems at 300°K, including the solute-solvent (B_{Kr-w}) and water "reorganization" (ΔU_{w-w}) components (Eq. 1). For the constant volume process ($\Delta V = 0.0$ Å^3), ΔH^*_{Kr} equals -6.3 ± 1.3 kcal/mol, and for the constant-pressure process ($\Delta V = 48.74$ Å^3) ΔH^*_{Kr} equals -3.4 ± 1.3 kcal/mol. As seen in Table 1, there is good agreement between the calculated ΔH^*_{Kr} at constant pressure with the experimental value of -3.3 kcal/mol, which was obtained under the same environmental conditions. Unfortunately, we are unaware of experimental data that can be compared for the constant-volume process. In contrast to ΔH^*_{Kr}, the solute-solvent interaction energy does not significantly change between the two processes. Its value is -5.43 ± 0.03 kcal/mol at constant volume and -5.40 ± 0.03 kcal/mol at constant pressure. Thus, the change in ΔH^*_{Kr} between the two process is primarily due to differences in the water "reorganization" energy, which is -0.9 ± 1.3 kcal/mol at constant volume, and 2.0 ± 1.3 kcal/mol at constant pressure. As seen in Fig. 4 *B*, similar ΔH^*_{Kr} values are calculated for the LJ water systems: i.e., -6.4 ± 0.5 kcal/mol at constant volume and

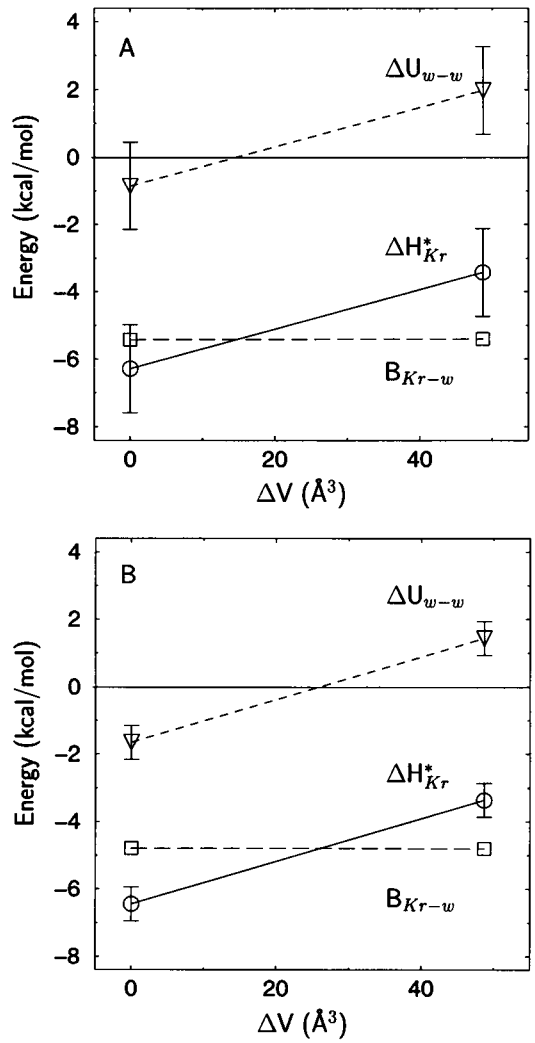

FIGURE 4 Calculated "solvation" enthalpy (ΔH^*_{Kr}) (○) of the (*A*) TIPS3P and (*B*) LJ water systems. The solute-solvent binding (B_{Kr-w}) (□) and water "reorganization" (ΔU_{w-w}) (▽) energy components are also shown. The constant volume process is at $\Delta V = 0$ Å^3, and the constant pressure process is at $\Delta V = 48.74$ Å^3.

-3.4 ± 0.5 kcal/mol at constant pressure. However, the solute-solvent interaction energy is found to be approximately 0.62 kcal/mol less negative than for the TIPS3P systems at both constant volume and constant pressure. This is easily explained by the smaller magnitude of the first peak in $g(r)_{Kr-w}$ for the LJ water systems (Fig. 1 *B*), which corresponds to a smaller number of water molecules in the first shell available to interact with the krypton atom. It is also seen, however, that this difference in B_{Kr-w} is compensated by an equal and opposite change in ΔU_{w-w}, which is due to the same reason and is responsible for the similar ΔH^*_{Kr} values between the TIPS3P and LJ water systems.

To examine the effects in more detail, Fig. 5 *A* plots the average potential energy of a TIPS3P water molecule as a function of distance from the solute. The data presented are specifically from the volume-adjusted Kr-containing system; however, the results from the constant-volume system are not

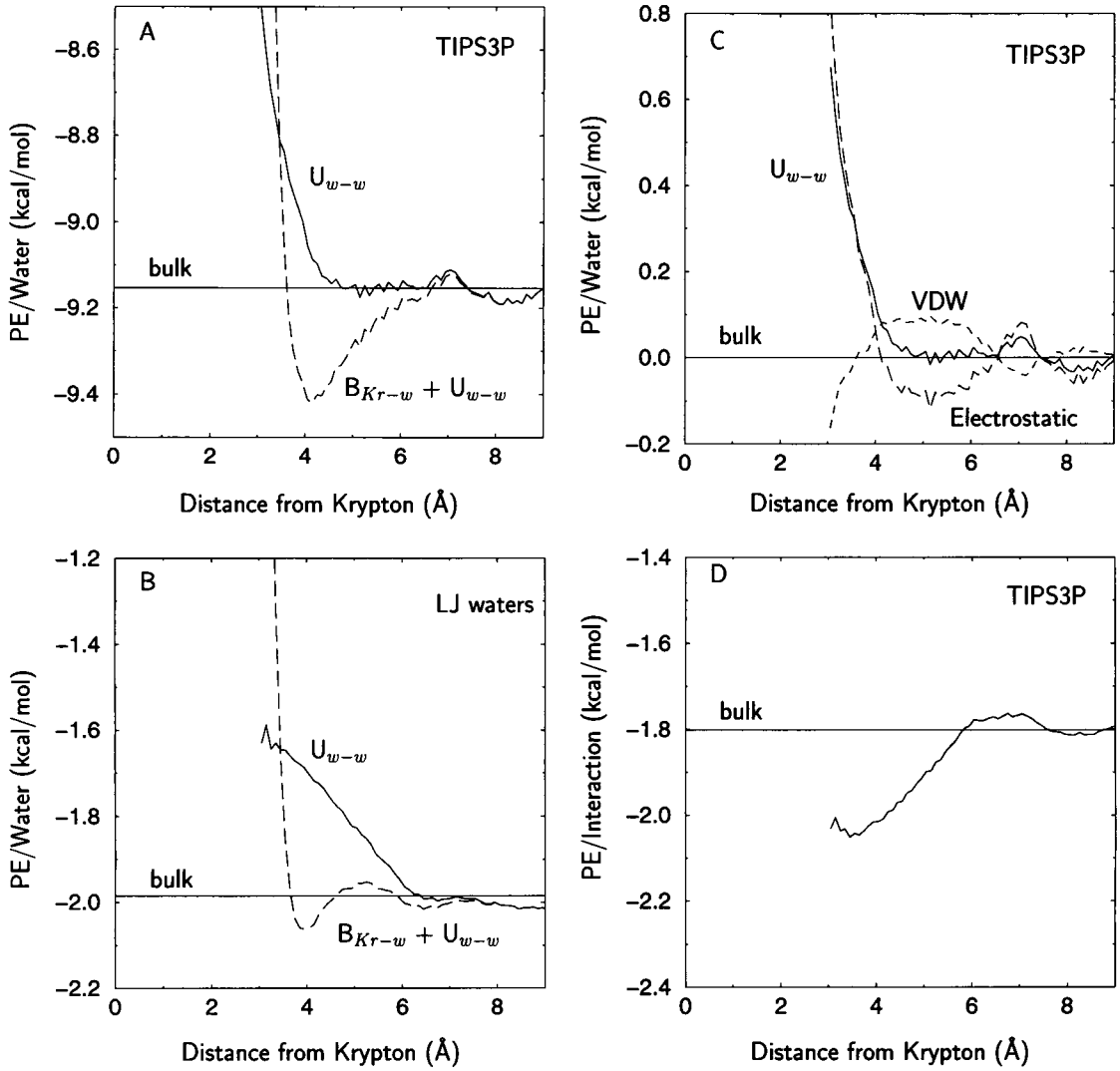

FIGURE 5 (*A–C*) Average potential energy per water molecule as a function of distance from the krypton atom. The solid line represents interactions with other water molecules only (U_{w-w}), and the dashed line includes the interaction with the solute to form the total potential energy ($B_{Kr-w} + U_{w-w}$). (*A*) TIPS3P system; (*B*) LJ water system; and (*C*) decomposition of U_{w-w} from the TIPS3P system into the electrostatic (*long dashed*) and VDW (*short dashed*) components. (*D*) Average energy per water-water interaction as a function of distance from the krypton atom, including only nearest neighbors, defined by being ≤4 Å apart. In *A*, *B*, and *D*, the horizontal line is the associated value calculated in the bulk phase; in *C* the line is an arbitrary common reference.

significantly different. The solid line shows the component due to interactions with other water molecules only (U_{w-w}), and the dashed line shows the total interaction energy, which includes the VDW interaction with the krypton ($B_{Kr-w} + U_{w-w}$). To show the deviation from the bulk phase, the average potential energy of a water molecule calculated from the pure TIPS3P system (−9.153 ± 0.004 kcal/mol) is plotted as a horizontal line. As can be seen from the U_{w-w} curve (solid line), the water-water interaction energy is most destabilized for molecules closest to the krypton and converges to the bulk value at a distance of ~4.3 Å. This involves only the closest 10 to 11 water molecules, which make up the first solvation shell. At 3.75 Å, which is the first peak of $g(r)_{Kr-w}$ and the region of highest density (Fig. 1 *B*), the destabilization is 0.22 kcal/mol per molecule, which is only ~2.5% of the unperturbed value. However, as seen by the total energy curve (*dashed line*), the VDW interaction with the solute overcompensates for this effect and enhances the stability of the water molecules from a distance of 3.6–6.5 Å. This is what is responsible for the favorable ΔH^*_{Kr} of the solvation process at 300°K (see Table 1). For comparison, Fig. 5 *B* shows the results from the LJ water systems. In this case, the destabilization of the water-water interaction energy is found to extend up to ~6.0 Å from the krypton, which is at the beginning of the second solvation shell (Fig. 1 *B*). At the peak of the first shell (3.75 Å), the destabilization is 0.31 kcal/mol per water molecule, which is ~50% more than for the TIPS3P waters.

The fact that the TIPS3P waters in the solvation shell are destabilized to a lesser degree than the LJ waters suggests that they are being partially stabilized by enhancement of hydrogen bond interactions. To further examine this effect, Fig. 5 *C* shows the electrostatic and

VDW components of the water-water interaction energy (U_{w-w}) of the TIPS3P waters from Fig. 5 *A*. To compare the relative degrees of perturbation, each curve has been shifted by subtracting the average value for that quantity obtained from the pure water simulation: i.e., −10.294 kcal/mol for the electrostatic component, 1.140 kcal/mol for the VDW component, and −9.153 kcal/mol for the sum of the two. For waters in the first solvation shell (~3.75 Å), the 0.22 kcal/mol per molecule destabilization is due primarily to a decrease in favorable electrostatic interactions. Between the first and second shells, at ~5.5 Å, the VDW energy is destabilized by ~0.1 kcal/mol per water, which is similar to the result for the LJ water systems (Fig. 5 *B*). However, this is compensated for in the TIPS3P water systems by a favorable enhancement of the electrostatic energy, which indicates a relatively small enhancement of the hydrogen bonding between water molecules. This is in fact what would be expected from the net orientational preferences observed for the waters in Fig. 2. As a better quantization of this effect, Fig. 5 *D* displays the energy per interaction as a function of distance from the krypton atom. The criterion for interaction was that the waters are within 4 Å of each other, which only includes the directly hydrogen bonded, nearest neighbors. As can be seen, each interaction is stabilized by a maximum of 0.25 kcal/mol at a distance of 3.45 Å, which is in the region of maximum angular orientational ordering (see Fig. 2). The involvement of the TIPS3P hydrogen bonds is confirmed by the absence of a similar effect in the LJ water systems (data not shown). However, this stabilization does not extend significantly to interactions with the next-nearest neighbors or beyond, which are not directly hydrogen bonded (data not shown). Thus, the fact that the net water-water energy per molecule (i.e., U_{w-w}) in the solvation shell is destabilized (Fig. 5 *A*) indicates that the stabilization due to angular ordering is overpowered by the loss of favorable interactions due to the excluded volume of the solute.

Finally, it is left to investigate why the calculated ΔH^*_{Kr} is more positive for the process at constant pressure than at constant volume. As seen in Fig. 4, this $\Delta\Delta H^*_{Kr}$ is 2.9 ± 1.8 kcal/mol for the TIPS3P water systems, and 3.1 ± 0.7 kcal/mol for the LJ water systems. Because the magnitude is approximately the same for the two water models, this cannot be related to the hydrogen bonding ability of regular water. To investigate this further, simulations of the pure TIPS3P water system were carried out using different cell sizes to determine the volume dependence of the water-water interaction energy. This was calculated to be 0.33 ± 0.04 cal/mol/Å^3 per molecule, which predicts a similar $\Delta\Delta H^*_{Kr}$ of 3.4 ± 1.3 kcal/mol for the 214 waters in the systems and the 48.74-Å^3 difference in volume. Thus, the difference in "solvation" enthalpy calculated for the two processes is primarily a global density effect, rather than being due to any exclusive change in the solvation shell.

Solvation free energy

Fig. 6, *A–D*, shows the thermodynamic integration results for the transfer of krypton into TIPS3P water at 300°K and constant volume using the paths described by Eqs. 4a–d. The points with error bars (±2σ) are the ensemble average values of the derivative at the specific value of lambda ($\langle \partial B(\lambda)/\partial\lambda \rangle_\lambda$). In each figure, the three dashed lines indicate the high and low range of the integration, which is obtained from the error bar-defined high and low range of the integrand curve (*solid line*). Because of the difficulty of propagating the error through the integration, the statistical uncertainty was taken to be the variation in the result at λ = 1.0. It should be noted, of course, that this neglects any error that may be introduced because of the quadrature approximation of the integrand (see Methods). The calculated "solvation" free energies for the four paths are 1.1 ± 0.7, 1.0 ± 0.6, 1.1 ± 0.6, and 1.1 ± 0.6 kcal/mol, respectively, which satisfy the test that the results be path independent (see Methods). Thus, all of the paths give a ΔG^*_{Kr} that is ~0.6 kcal/mol less than the experimentally determined value of 1.68 kcal/mol (Table 1), which is just at the limit of the estimated uncertainty. For the LJ water system the corresponding results are −0.2 ± 0.5, −0.2 ± 0.4, −0.2 ± 0.5, and 0.0 ± 0.4 kcal/mol, which are also the same within the statistical uncertainty. Thus, unlike the more realistic TIPS3P waters, the solvation of krypton is found to be slightly thermodynamically favored in the LJ liquid.

As described by Resat and Mezei (1993), the path of Eq. 4a (Fig. 6 *A*) results in a nearly linear integrand, which helps to reduce error potentially introduced by the quadrature approximation of the integrand (see Methods). For this reason, only a 0.2 instead of a 0.1 sampling interval was used in the 0.2 to 1.0 range of λ. Because the integrand appeared to be curving in the below 0.2 region, ensemble averages were additionally calculated at λ = 0.001, 0.005, 0.01, and 0.1. The results for the smallest two of these are 4.8 ± 3.7 and 5.4 ± 1.7 kcal/mol, and are not shown in the figure for reasons of clarity. However, because the $\Delta\lambda$ is very small, the inclusion of these points provides only a negligible correction to the assumption that the integrand is constant from λ = 0.1 → 0.0. A similar situation occurs for the separation-shifted scaled path (Eq. 4d) displayed in Fig. 6 *D*, in which the missing calculated values at λ = 0.001 and 0.005 are 29.160 and 24.585 kcal/mol. As discussed in the Methods, the second and third polynomial paths (Eqs. 4b, c) were chosen to "stretch out" the lower region of λ and thus provide ensemble averages at smaller effective sizes of the solute. The result of this is best seen in Fig. 6 *C*, in which the integrand is effectively zero until λ = 0.6, at which point the effective radius of the solute is ~0.7 Å. When λ = 0.1 with this path, the effective radius reduces to only 0.0017 Å. The fact that all four paths give the same ΔG^*_{Kr} suggests that the calculations are not falling prey to numerical convergence problems.

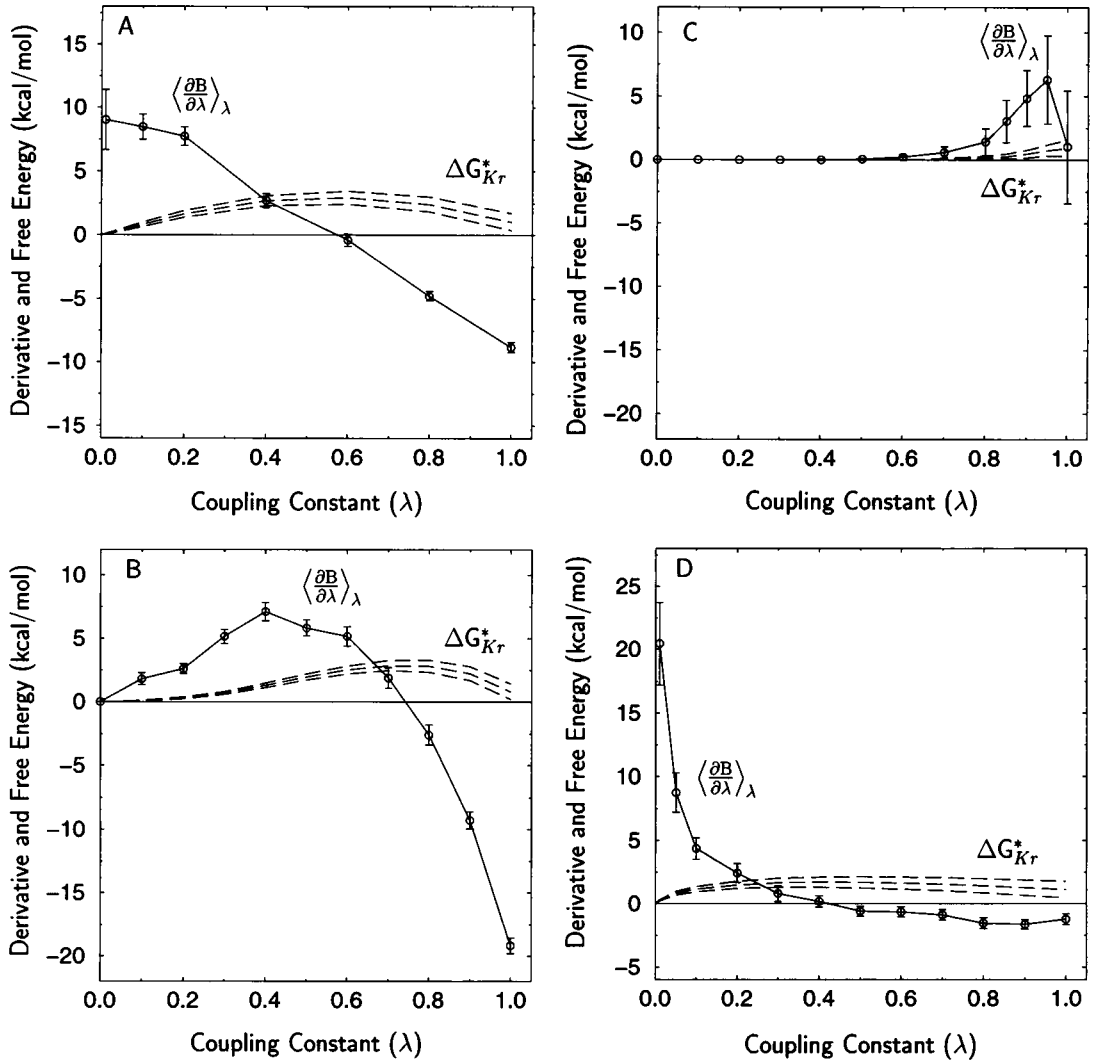

FIGURE 6 Thermodynamic integration of krypton "grown" in the constant-volume TIPS3P water system. (*A–D*) Results from the paths of Eqs. 4a–d, respectively. The solid line is the quadrature-approximated ensemble average derivative of the solute-solvent binding energy as a function of lambda ($\langle \partial B(\lambda)/\partial\lambda \rangle_\lambda$). The dashed lines indicate the high and low range of the "solvation" free energy (ΔG^*_{Kr}) integral obtained from the error bar-defined ($\pm 2\sigma$) range of the derivative curve.

Solvation entropy

As described in the Methods, the "solvation" entropy (ΔS^*_{Kr}) was determined simply from the calculated ΔG^*_{Kr} and ΔH_{Kr} values using Eq. 3. The results for the TIPS3P and LJ water systems at constant volume and constant pressure are presented in Table 3. Comparison with Table 1 shows that the calculated ΔS^*_{Kr} of -15 ± 5 cal/mol/K for the TIPS3P system at constant pressure and 300°K agrees well with the experimental value of -16.5 cal/mol/K (which is for the same conditions). This is in contrast to the process at constant volume, in which the calculated value of -25 ± 5 cal/mol/K is significantly more negative and thus even more unfavorable. As seen in Table 3, it is this ~10 cal/mol/K ($\times$ 300°K) difference in the "solvation" entropy that nearly counteracts the 2.9 kcal/mol difference in the "solvation" enthalpy between the two processes to provide the nearly equal "solvation" free energy values (see Methods). Similar results are obtained for the LJ water systems, in which the calculated ΔS^*_{Kr} is found to be only $\sim 4.5 \pm 6$ cal/mol/K less negative than for the corresponding TIPS3P systems (i.e., -10 ± 3 cal/mol/K at constant pressure and -21 ± 3 cal/mol/K at constant volume). It should be noted that these results agree (within the statistical uncertainty) with the change in entropy calculated for the constant-pressure process using an alternative formalism based on the solute-solvent distance and orientation correlations (Paulaitis et al., 1994).

DISCUSSION

The importance of using large time-scale simulations to calculate the "solvation" enthalpy is illustrated in Fig. 3. As described above, statistical uncertainty is a problem in this calculation because the difference in average potential en-

TABLE 3 Calculated values of the "solvation" free energy (ΔG^*_{Kr}), enthalpy (ΔH^*_{Kr}), and entropy (ΔS^*_{Kr}) of krypton in TIPS3P and LJ liquids at 300°K

	ΔG^*_{Kr} (kcal/mol)	ΔH^*_{Kr} (kcal/mol)	ΔS^*_{Kr} (cal/mol/K)
TIPS3P waters			
Const. *V*	1.1 (0.6)	−6.3 (1.3)	−25 (5)
Const. *P*	1.1 (0.6)	−3.4 (1.3)	−15 (5)
LJ waters			
Const. *V*	−0.2 (0.4)	−6.4 (0.5)	−21 (3)
Const. *P*	−0.2 (0.4)	−3.4 (0.5)	−10 (3)

The values in parentheses are the statistical uncertainty (2σ). The values for the "solvation" free energy at constant pressure were taken to be the same as that calculated at constant volume (see Methods).

ergy between the Kr-containing and pure water systems is relatively small compared to the magnitude of the fluctuations. For example, it takes approximately 100 ps worth of sampling for the error bars of the two running averages to separate, and thus to calculate a ΔH^*_{Kr} at least significantly different from zero. In this case, it was required to run the TIPS3P simulations approximately 10 times longer to reduce the uncertainty to an acceptable level. Unfortunately, this strategy has diminishing returns, because the error depends on the inverse of the square root of the simulation time (Eq. 5). Thus, doubling the time to 2 ns would provide only another $1/\sqrt{2}$ factor reduction in the uncertainty. Another strategy is to decrease the fluctuations by increasing the number of water molecules in the system (Haile, 1992). Unfortunately, this also has diminishing returns, because the same inverse square root relation exists between the error and the system size, and the additional number of waters increases the required amount of computing time.

Perhaps the most significant result from the "solvation" enthalpy calculations is that the interaction energy between the water molecules (U_{w-w}) in the solvation shell is destabilized compared to that in the bulk phase (Fig. 5 *A*). This is contrary to the classical "iceberg" model, which predicts a substantial stabilization of the hydrogen bond interactions. Rather, the negative ΔH^*_{Kr} (i.e., release of heat) observed at room temperature (Table 1) is due mostly to the overridingly favorable solute-solvent VDW interaction. A similar conclusion has been made by Jorgensen et al. (1985), based on Monte Carlo simulations of hydrophobic hydration comparing solutes of different sizes. The source of the destabilization of U_{w-w} in the TIPS3P water systems can be better understood from analysis of the LJ water systems (Fig. 5 *B*). Because the LJ water model lacks the ability to form tetrahedral hydrogen bond structures, the effects in those systems must be due solely to perturbation of the VDW interactions. In the first solvation shell, which peaks at 3.75 Å, the loss of favorable water-water VDW energy is attributed primarily to the excluded volume of the solute, which partially shields the waters and thus reduces the extent of contact each water molecule makes with other water molecules. Similarly, the smaller degree of destabilization between the first and second shells, at ~5.5 Å, is attributed to the reduction in density seen in $g(r)_{Kr-w}$ (Fig. 1 *B*). Because the LJ water model has the same effective size and leads to the same calculated ΔH^*_{Kr}, it is assumed that these packing constraints equally affect the energy of the TIPS3P waters. Thus, the approximately 30% reduction in the destabilization of U_{w-w} observed for the TIPS3P waters (comparing Fig. 5, *A* and *B*) must be due to a small amount of counteracting "iceberg"-like enhancement of the hydrogen bond interactions. This is more clearly demonstrated in Fig. 5, *C* and *D*. Specifically, in Fig. 5 *C* the ~0.1 kcal/mol destabilization of the VDW interaction in the intershell region at ~5.5 Å (which is the same for the LJ waters shown in Fig. 5 *B*) is found to be equally compensated for by an enhancement of the favorable electrostatic interaction (which is the largest component of the hydrogen bond energy). Similarly, Fig. 5 *D* shows that for waters in the first solvation shell the average interaction with a nearest neighbor is stabilized by as much as 0.25 kcal/mol. It should be noted, however, that these values represent only a minor perturbation of the full hydrogen bond energy, which is on the order of −6 kcal/mol.

Finally, the classical "iceberg" model attributes the reduction in entropy for the solvation process at room temperature primarily to the loss of rotational freedom of the water molecules in the solvation shell. Indeed, as Fig. 2 demonstrates, the orientation of the TIPS3P water molecules is effected up to a distance of ~6 Å from the solute. However, the fact that the ΔS^*_{Kr} for the LJ systems is found to be a large percentage of that calculated for the TIPS3P systems (see Table 3) indicates that rotational constraint cannot be the major factor. A similar conclusion was arrived at by Madan and Lee (1994), based on the calculated free energy of cavity formation in similar model liquids. As discussed above, the LJ model is spherically symmetrical and thus does not have a definable orientation with respect to the solute or other water molecules. Therefore, the ΔS^*_{Kr} calculated for the LJ systems can only be due to changes associated with the translational motion of the water molecules. It is easy to envision how addition of the bulky solute has the effect of reducing the number of ways in which the water molecules can be translationally arranged throughout the volume of the system. Thermodynamically, this would be described as decreasing the number of complexions (Ω) of the system ($S = k_b \ln \Omega$). As discussed in the Methods, the volume available to the water molecules remains approximately constant for the transfer process at constant pressure. Thus, the reduction in entropy for this system reflects only the exclusion of the waters from the region occupied by the solute. The additional ~10.5 cal/mol/K decrease in S^*_{Kr} that occurs for the process at constant volume is therefore due to the 48.74 Å^3 reduction in effective volume available to the solvent molecules. The fact that the magnitude of this change is the same for the LJ and TIPS3P water systems indicates that it is not due to compression of the pseudotetrahedral hydrogen bonding structure of regular water. Rather, the component of ΔS^*_{Kr} that is due to hydrogen bonding in the TIPS3P systems is obtained

from subtracting the value calculated for the LJ water systems. As seen in Table 3, this ~4.5 cal/mol/K amount represents only 30% of the total for the process at constant pressure, and only 18% at constant volume.

The authors would like to thank Drs. Byungkook Lee and Bernard R. Brooks for their insightful discussions. We also would like to express our appreciation to the Frederick Biomedical Supercomputer Center of the National Cancer Institute for the grant of computing resources.

REFERENCES

Allen, M. P., and D. J. Tildesley. 1987. Computer Simulation of Liquids. Clarendon Press, Oxford.

Ben-Naim, A. 1987. Solvation Thermodynamics. Plenum Press, New York.

Ben-Naim, A. 1992. Statistical Thermodynamics of Chemists and Biochemists. Plenum Press, New York.

Beveridge, D. L., and F. M. DiCapua. 1989. Free energy via molecular simulation: applications to chemical and biomolecular systems. *Annu. Rev. Biophys. Biophys. Chem.* 18:431–492.

Blokzijl, W., and J. B. F. N. Engberts. 1993. Hydrophobic effects. Opinions and facts. *Angew. Chem. Int. Ed. Engl.* 32:1545–1579.

Brooks, B. R., R. E. Bruccoleri, B. D. Olafson, D. J. States, S. Swaminathan, and M. Karplus. 1983. CHARMM: a program for macromolecular energy, minimization, and dynamics calculations. *J. Comput. Chem.* 4:187–217.

Cross, A. J. 1986. Influence of Hamiltonian parameterization on convergence of Kirkwood free energy calculations. *Chem. Phys. Lett.* 128: 198–202.

Crovetto, R., R. Fernández-Prini, and M. L. Japas. 1982. Solubilities of inert gases and methane in H_2O and in D_2O in the temperature range of 300 to 600 K. *J. Chem. Phys.* 76:1077–1086.

Dill, K. A. 1990. Dominant forces in protein folding. *Biochemistry.* 29: 7133–7155.

Fleischman, S. H., and D. A. Zichi. 1991. Free energy simulations of methane solvation: a study of integrand convergence properties using thermodynamic integration. *J. Chim. Phys.* 88:2617–2622.

Forsman, J., and B. Jönsson. 1994. Monte Carlo simulations of hydrophobic interactions: a test particle approach. *J. Chem. Phys.* 101: 5116–5125.

Frank, H. S., and M. W. Evans. 1945. Free volume and entropy in condensed systems. III. Entropy in binary liquid mixtures; partial molal entropy in dilute solutions; structure and thermodynamics in aqueous electrolytes. *J. Chem. Phys.* 13(11):507–532.

Haile, J. M. 1992. Molecular Dynamics Simulations: Elementary Methods. John Wiley and Sons, New York.

Holtzer, A., and M. F. Emerson. 1969. On the utility of the concept of water structure in the rationalization of the properties of aqueous solutions of proteins and small molecules. *J. Phys. Chem.* 73:26–33.

Jorgensen, W. L., J. Chandrasekhar, J. D. Madura, R. W. Impey, and M. L. Klein. 1983. Comparison of simple potential functions for simulating liquid water. *J. Chem. Phys.* 79:926–935.

Jorgensen, W. L., J. Gao, and C. Ravimohan. 1985. Monte Carlo simulations of alkanes in water: hydration numbers and the hydrophobic effect. *J. Phys. Chem.* 89:3470–3473.

Krynicki, K., C. D. Green, and D. W. Sawyer. 1978. Pressure and temperature dependence of self-diffusion in water. *Faraday Discuss. Chem. Soc.* 66:199–208.

Lazaridis, T., and M. E. Paulaitis. 1992. Entropy of hydrophobic hydration: a new statistical mechanical formulation. *J. Phys. Chem.* 96:3847–3855.

Madan, B., and B. Lee. 1994. Role of hydrogen bonds in hydrophobicity: the free energy of cavity formation in water models with and without the hydrogen bonds. *Biophys. Chem.* 51:279–289.

Mezei, M. 1992. Polynomial path for the calculation of liquid state free energies from computer simulations tested on liquid water. *J. Comput. Chem.* 13:651–656.

Mezei, M. 1993. Calculation of solvation free-energy differences for large solute change from computer simulations with quadrature-based nearly linear thermodynamic integration. *Mol. Simulation.* 10:225–239.

Mezei, M., and D. L. Beveridge. 1986. Free energy simulations. *In* Computer Simulations and Biomolecular Systems. D. L. Beveridge and W. L. Jorgenson, editors. *Ann. N.Y. Acad. Sci.* 482:1–23.

Pastor, R. W., B. R. Brooks, and A. Szabo. 1988. An analysis of the accuracy of Langevin and molecular dynamics algorithms. *Mol. Phys.* 65(6):1409–1419.

Paulaitis, M. E., H. S. Ashbaugh, and S. Garde. 1994. The entropy of hydration of simple hydrophobic solutes. *Biophys. Chem.* 51:349–357.

Pratt, L. R., and A. Pohorille. 1992. Theory of hydrophobicity: transient cavities in molecular liquids. *Proc. Natl. Acad. Sci. USA.* 89:2995–2999.

Prevost, M., D. van Belle, G. Lippens, and S. Wodak. 1990. Computer simulations of liquid water: treatment of long-range interactions. *Mol. Phys.* 71:587–603.

Ravishanker, G., and D. L. Beveridge. 1986. Theoretical studies of the hydrophobic effect. *In* Studies in Physical and Theoretical Chemistry. 41: Theoretical Chemistry of Biological Systems. G. Náray-Szabö, editor. Elsevier, Amsterdam. 423–493.

Resat, H., and M. Mezei. 1993. Studies on free energy calculations. I. Thermodynamic integration using a polynomial path. *J. Chem. Phys.* 99:6052–6061.

Resat, H., and M. Mezei. 1994. Studies on free energy calculations. II. A theoretical approach to molecular solvation. *J. Chem. Phys.* 101: 6126–6140.

Simonson, T. 1993. Free energy of particle insertion: an exact analysis of the origin singularity for simple liquids. *Mol. Phys.* 80:441–447.

Steinbach, P. J., and B. R. Brooks. 1994. New spherical-cutoff methods for long-range forces in macromolecular simulation. *J. Comput. Chem.* 15:667–683.

Swope, W. C., and H. C. Andersen. 1984. A molecular dynamics method for calculating the solubility of gases in liquids and the hydrophobic hydration of inert-gas atoms in aqueous solution. *J. Phys. Chem.* 88: 6548–6556.

Watanabe, K., and H. C. Andersen. 1986. Molecular dynamics study of the hydrophobic interaction in an aqueous solution of krypton. *J. Phys. Chem.* 90:795–802.

Wallqvist, A., and B. J. Berne. 1993. Effective potentials for liquid water using polarizable and nonpolarizable models. *J. Phys. Chem.* 97: 13841–13851.

Wallqvist, A., and D. G. Covell. 1996. On the origins of the hydrophobic effect: observations from simulations of n-Dodecane in model solvents. *Biophys. J.* 71:600–608.

Wallqvist, A., and O. Teleman. 1991. Properties of flexible water models. *Mol. Phys.* 74:515–533.

Young, L., R. L. Jernigan, and D. G. Covell. 1994. A role for surface hydrophobicity in protein-protein recognition. *Protein Sci.* 3:717–729.

Zacharias, M., T. P. Straatsma, and J. A. McCammon. 1994. Separation-shifted scaling, a new scaling method for Lennard-Jones interactions in thermodynamic integration. *J. Chem. Phys.* 100:9025–9031.

Zichi, D. A., and P. J. Rossky. 1985. The equilibrium solvation structure for the solvent-separated hydrophobic bond. *J. Chem. Phys.* 83: 797–808.

Zichi, D. A., and P. J. Rossky. 1986. Solvent molecular dynamics in regions of hydrophobic hydration. *J. Chem. Phys.* 84:2814–2822.